Comparative Study for Identification of Feeding Arteries of Hepatocellular Carcinoma by 3D Reformatted CT Angiography and Digital Subtraction Angiography during Transcatheter Arterial Chemoembolization (TACE)

Mohamed Sami Abdelhamed[1*], Fatma Anas Elsharawy[1], Mohamed Ahmed Youssef[1], Hazem Omar[2]
[1]Department of Radiodiagnosis, Faculty of Medicine, Tanta University, Gharbia, Egypt
[2]Department of Diagnostic Medical Imaging and Interventional Radiology,
National Liver Institute, Menoufia University, Menoufia, Egypt
***Corresponding author:** Mohamed Sami Abdelhamed, **Mobile:** (+20) 01001807190, **Email:** dr.msami1991@gmail.com

ABSTRACT
Background: The main treatment of intermediate-stage hepatocellular carcinoma (HCC) is considered to be transcatheter arterial chemoembolization (TACE). **Objective:** To compare the accuracy of 3D reformatted computed tomography (CT) angiography and digital subtraction angiography (DSA) during TACE for the identification of feeding arteries of hepatocellular carcinoma. **Patients and Methods:** This prospective study was performed on 50 cases already diagnosed with HCC. Arterial phase multidetector-row CT (MDCT) images were retrospectively reformatted and analyzed to determine the anatomical variants of hepatic arterial supply and tumor-feeding vessel using maximum intensity projection (MIP), multi-planar reconstruction (MPR), and volume-rendering (VR) technique and compared to results of DSA done during TACE. **Results:** The whole number of HCC lesions was 68 lesions. The accuracy of CT angiography using MIP and VR techniques for assessing hepatic artery variations was (100%) in MIP and (94%) in VR technique compared to DSA done during TACE. The total number of feeding arteries was 96 feeder arteries; 93 feeders were from hepatic artery branches and only 3 feeders were extra-hepatic. The accuracy of assessing the feeding arteries of HCC was (87.5%) in MIP and (24%) in VR techniques compared to DSA results. **Conclusions:** For evaluating HCC feeding arteries, CT angiography with MIP demonstrated more accuracy and superior image quality than the VR technique compared with DSA done during TACE.
Keywords: CT angiography, DSA, HCC, Transcatheter arterial chemoembolization (TACE).

INTRODUCTION
Hepatocellular carcinoma (HCC) is the sixth most frequent cancer worldwide. HCC is the sixth most common cancer in females and the second most common cancer in males in Egypt [1]. About one-third of cirrhotic individuals will develop HCC in their lifespan as it is the most significant risk factor for HCC [2]. Cirrhotic livers account for approximately 80% of all HCCs [3,4]. The most often used staging approach is the Barcelona Clinic Liver Cancer Staging (BCLC) system, which takes into consideration the extent of tumour, liver function, and health condition [5]. According to the BCLC algorithm, the main treatment for intermediate-stage HCC is transcatheter arterial chemoembolization (TACE) [6]. Chemoembolization of HCC is conducted by occluding the tumor-supplying artery or arteries following intra-arterial injection of a chemotherapeutic drug. The purpose of chemoembolization is to concentrate the antineoplastic agent in the tumor and induce tumor ischemia, therefore decreasing the systemic toxicity of the antineoplastic drug [6,7]. The effectiveness of the treatment depends on the selective injection of chemotherapeutic agents into the tumor-supplying artery or arteries. It has been found that performing ultra-selective TACE in the distal region of the subsegmental hepatic artery reduces the occurrence of adverse effects and improves local control [8].

Before performing superselective TACE, it is necessary to identify the feeding artery of the HCC. Digital subtraction arteriography (DSA) does not create three-dimensional images, and it is necessary to get several selective injections and oblique projections during TACE to locate feeding arteries. However, these methods increase the contrast volume provided, procedure duration, and radiation exposures [9].

Spatial and temporal resolutions have increased with the introduction of MDCT scanners, enabling the identification of tiny HCCs and feeding arteries present in the hepatic parenchyma around HCCs [10,11]. As a result, MDCT angiography combined with 3D imaging has become the dominant imaging approach for examining arteries [12]. Our objective was to compare the accuracy of 3D reformatted CT angiography and DSA done during TACE to identify feeding arteries of hepatocellular carcinoma.

PATIENTS AND METHODS
This prospective study was performed on 50 patients who were diagnosed with HCC (intermediate stage) according to Barcelona Clinic Liver Cancer (BCLC) guidelines and had the decision of the oncology committee to do intervention management (TACE). The patients attended to Radiodiagnosis and Medical Imaging Department, Tanta University Hospitals, and Diagnostic Medical Imaging and Intervention Radiology Department, National Liver Institute, Menoufia University during the period from November 2019 to October 2022.

The inclusion criteria were Child-Pugh class A or early B patients with HCC lesions not exceeding 50% of liver parenchyma, with no vascular or biliary invasion, and not fit or refuse surgery.

The exclusion criteria included Child-Pugh class late B or C, vascular or biliary invasion or distant metastasis, pregnancy, patients with bleeding tendency, allergy to contrast media, and serum creatinine level of more than 2 mg/dl.

Received: 01/10/2023
Accepted: 01/12/2023

All cases underwent full history taking, general examination to assess the general condition of the patient, laboratory investigation including complete blood count, bleeding profile, liver and renal function tests, and international normalized ratio (INR), and radiological investigations including ultrasound examination of the liver, Triphasic CT study of the liver with 3D reconstruction and DSA done during TACE for management of HCC.

Triphasic CT protocol

A 128 multidetector CT (SOMATOM, Siemens Healthcare, Germany) was used to scan all the cases. Before being scanned, cases were needed to fast for six hours and drink 800 to 1,000 cc of water. The patients were placed in a supine position, headfirst, arms lifted above the head. The scanning region ranged from the tracheal carina to the symphysis pubis. All individuals were subjected to craniocaudal scanning during a single breath hold. A non-contrast upper abdominal scan was used to determine the location of HCC. After that, a dosage of 1.5 ml/kg body weight nonionic contrast material with a concentration of 370 mg of iodine per milliliter (Ultravist 370) was given intravenously in the right antecubital vein at a rate of 4-5 mL/sec using an automated injector using a 19-gauge catheter. To perform optimal arterial phase MDCTA scans, an automatic bolus-triggering software program was systematically used with a circular region of interest positioned within the abdominal aorta above the level of celiac artery bifurcation, and the threshold for triggering data acquisition was set at 100 HU to determine the delay in scanning for arterial phase imaging. This arterial phase imaging was conducted around 25-30 seconds following the commencement of contrast injection, as determined by the triggering software. The following scanning settings were utilized: detector collimation, 128 x 0.625 mm on 128-MDCT; tube current, 120 kilovolts (peak); 200 mA; reconstruction increment, 3 mm with 3-mm-thick sections; section width, 3 mm. The raw data from the MDCT arterial phase scan was used to obtain additional 1-mm-thick images.

Transcatheter arterial chemoembolization (TACE):

Cases fasted the night before the technique and were hospitalized the morning of the procedure. Peripheral pulses and blood pressure were monitored. Random blood sugar was measured.

Chemoembolization was conducted percutaneously while the patient was awake in the angiography suite (Allura Xper; Philips Medical Systems). Following local anaesthetic infiltration, Seldinger's method was used to puncture the common femoral artery. A 5-French vascular sheath was placed over a 0.035-inch guidewire in the common femoral artery. Under fluoroscopic guidance, a 5-French Cobra head catheter was inserted into the descending abdominal aorta over the guidewire and used to determine the celiac axis. Diagnostic visceral arteriography was done. A celiac arteriogram was done to rule out any structural variation and assess the anatomical distribution of the celiac trunk. The volume of contrast media was 20 cc injected and films were taken at a rate of 2 films/sec. The celiac arteriogram guided the selective catheterization of the hepatic artery. The catheter was then pushed into the preferred hepatic artery branch, depending on the position of the tumour, which was recognised and noted by the arterial brush. Chemoembolization consisted of 50 mg Adriamycin mixed with 10 ml lipiodol and vigorous mixing to form a chemo-lipiodol mixture. The chemo-lipiodol combination was progressively delivered through the catheter using the free flow approach over a three-minute period under fluoroscopic supervision. This was followed by the insertion of gelatin sponge particles under fluoroscopic control. The goal of arterial embolization was to remove tumour blush from hepatic arteriography conducted soon after chemoembolization. The catheter and introducer sheath were removed, and adequate compression of the puncture site was maintained for 10-15 minutes.

Image analysis:

For post-processing and analysis, image data were transmitted to the local workstation (Philips Extended Brilliance workspace workstation, Philips Medical Systems, Netherlands) and picture archiving and communication system (PACS). To reconstruct the hepatic artery and perihepatic arteries, thin-slice images were utilized with techniques including curved planar reconstruction (CPR), MIP, and VR.

Distal subtraction angiography (DSA) images were defined as the criterion standard. To evaluate the tumor-feeding vessel, after that DSA images were compared to VRT and MIP images. The case was classed as positive if the tumor-feeding vessel on VRT or MIP matched that on DSA; otherwise, it was labeled as negative. In addition, the anatomical categorization of hepatic arteries was examined by comparing DSA images with MIP and VRT images based on Michel's classification.

Ethical approval:

This study was approved by the Ethics Committee of Tanta University Hospitals [Approval No. 33309/08/2019]. An informed written consent was obtained from the participants. The Helsinki Declaration was observed throughout the study's duration.

Statistical analysis:

SPSS version 26.0 was used to statistically analyze the data. The histograms and Shapiro-Wilk test were utilized to determine the normality of the data distribution. Qualitative variables were presented as frequency and percentage (%). Quantitative parametric variables were displayed as mean±standard deviation (SD). A significant p-value was defined as one that is equal to or less than 0.05.

RESULTS

We included 50 cases, 11 females and 39 males, their mean age was 61.9 ± 8.4 years **(Table 1).**

Table (1): Demographic data of the studied patients

		n=50
Age (Year)	Mean ± SD	61.9 ± 8.4
	<50	4 (8%)
	50 - <60	15 (30%)
	60 - <70	21 (42%)
	> 70	10 (20%)
Sex	Male	39 (78%)
	Female	11 (22%)

The majority of cases (76%) presented with solitary lesions with a predilection of right lobe affection. The total number of examined HCC lesions was 68 lesions; the distribution of examined lesions according to the number of segments involved, size of the lesion, and history of previous management are detailed in Table 2. Regarding the segmental distribution of examined focal lesions; the most affected segment was segment VIII and the least affected segment was Segment I**.**

Table (2): Characters and hepatic segmental distribution of the lesions among the studied patients

		N of patients= 50
Number of lesions	One lesion	38 (76%)
	Two lesions	6 (12%)
	Three lesions	6 (12%)
Site of lesions	Right lobe	30 (60%)
	Left lobe	11 (22%)
	Bi-lobar	8 (16%)
	Caudate lobe	1 (2%)
		N of lesions = 68
Number of segments affected	One segment	56 (82.4%)
	Two segments	9 (13.2%)
	Three segments	3 (4.4 %)
Size of lesions	< 3cm	13 (19.1%)
	≥ 3cm and < 5cm	26 (38.2%)
	≥ 5cm and < 10cm	24 (35.3%)
	≥ 10cm	5 (7.4%)
Previous management	De-novo lesion	52 (76.5%)
	Previously chemo-embolized	16 (23.5%)
Segments affected	I	2 (2.9%)
	II	3 (4.4%)
	III	9 (13.2%)
	IV	10 (14.7%)
	V	5 (7.4%)
	VI	5 (7.4%)
	VII	8 (11.7%)
	VIII	14 (20.6%)
	V and VIII	3 (4.4%)
	VI and VII	4 (5.9%)
	VII and VIII	1 (1.5%)
	V and VI	1 (1.5%)
	VI, VII and VIII	3 (4.4%)

Data are presented as frequency (%).

Regarding the type of hepatic arterial supply (Michel's classification) assessed by DSA, MIP, and VR, the number of patients who had classic hepatic arterial supply (Type I) was 36 (72%), while the number of patients who had anatomical variants was 14 (28%), with type III being the most anatomical variant in studied patients. Regarding the accuracy of assessment of anatomical classification of hepatic artery compared to DSA, the accuracy of MIP was 100% and that of VR was 94%. Two cases with type II were assessed by VR as normal anatomy (Type I) and the case with type VIII was assessed by VR as type II **(Table 3).**

Table (3): Distribution of the studied patients according to the type of hepatic arterial supply (Michel's classification) assessed by DSA, MIP, and VR

Michel's classification	n=50			P value
	DSA*	MIP	VR	
Type I	36 (72%)	36 (72%)	38 (76%)	0.873
Type II	4 (8%)	4 (8%)	3 (6%)	0.907
Type III	6 (12%)	6 (12%)	6 (12%)	---
Type IV	1 (2%)	1 (2%)	1 (2%)	---
Type VIII	1 (2%)	1 (2%)	0 (0%)	0.602
Type IX	2 (4%)	2 (4%)	2 (4%)	---

Data are presented as frequency (%). DSA*: Digital subtraction angiography was defined as the criterion standard. MIP: maximum intensity projection. VR: volume-rendering. Michel's classification: Type I, normal anatomy. Type II replaced left hepatic artery from left gastric artery. Type III replaced right hepatic artery from superior mesenteric artery. Type IV replaced both left and right hepatic arteries. Type VIII replaced left hepatic artery with accessory right hepatic artery, Type IX replaced common hepatic artery from the superior mesenteric artery**.**

The total number of feeder arteries of the 68 examined focal lesions was 96 feeder arteries; the majority of lesions 48 (70.6%) had only one feeder artery. Regarding the source of feeder arteries of examined lesions; the majority of feeder arteries (96.9%) were from branches of the hepatic artery.

The two lesions in segment I showed variable supply; one lesion was supplied by a single feeder artery from LHA and the other was supplied by two feeder arteries from RHA and RPHA. Segment IV showed 10 lesions; 5 lesions were supplied from the segment IV artery that originated from LHA and 4 lesions were supplied from the segment IV artery that originated from RHA and one lesion had an extra-hepatic supply from LIMA **(Table 4).**

Table (4): The number and the origin of feeder arteries assessed by DSA during TACE among the studied lesions.

	No. (%)
No. of feeder arteries (N of lesions=68)	
One feeder	48 (70.6%)
Two feeders	14 (20.6%)
More than two feeders	6 (8.8%)
Origin of feeder arteries (N of feeders=96)	
Left hepatic artery (LHA)	21 (21.9%)
Right hepatic artery (RHA)	5 (5.2%)
Right anterior hepatic artery (RAHA)	35 (36.5%)
Right posterior hepatic artery (RPHA)	32 (33.3%)
Right inferior phrenic artery (RIPA)	2 (2.1%)
Left internal mammary artery (LIMA)	1 (1%)

Data are presented as numbers (%).

Regarding the accuracy of assessing the tumour feeding arteries by MIP and VR in comparison with the findings of DSA, MIP was significantly accurate more than VR in the assessment of tumor-feeding arteries (**Table 5).**

Table (5): Assessment of tumor-feeding arteries by MIP and VR compared with DSA findings among the studied lesions.

	MIP	VR	P value
Positive	84	23	<0.001*
Negative	12	73	
Accuracy	87.5%	24%	

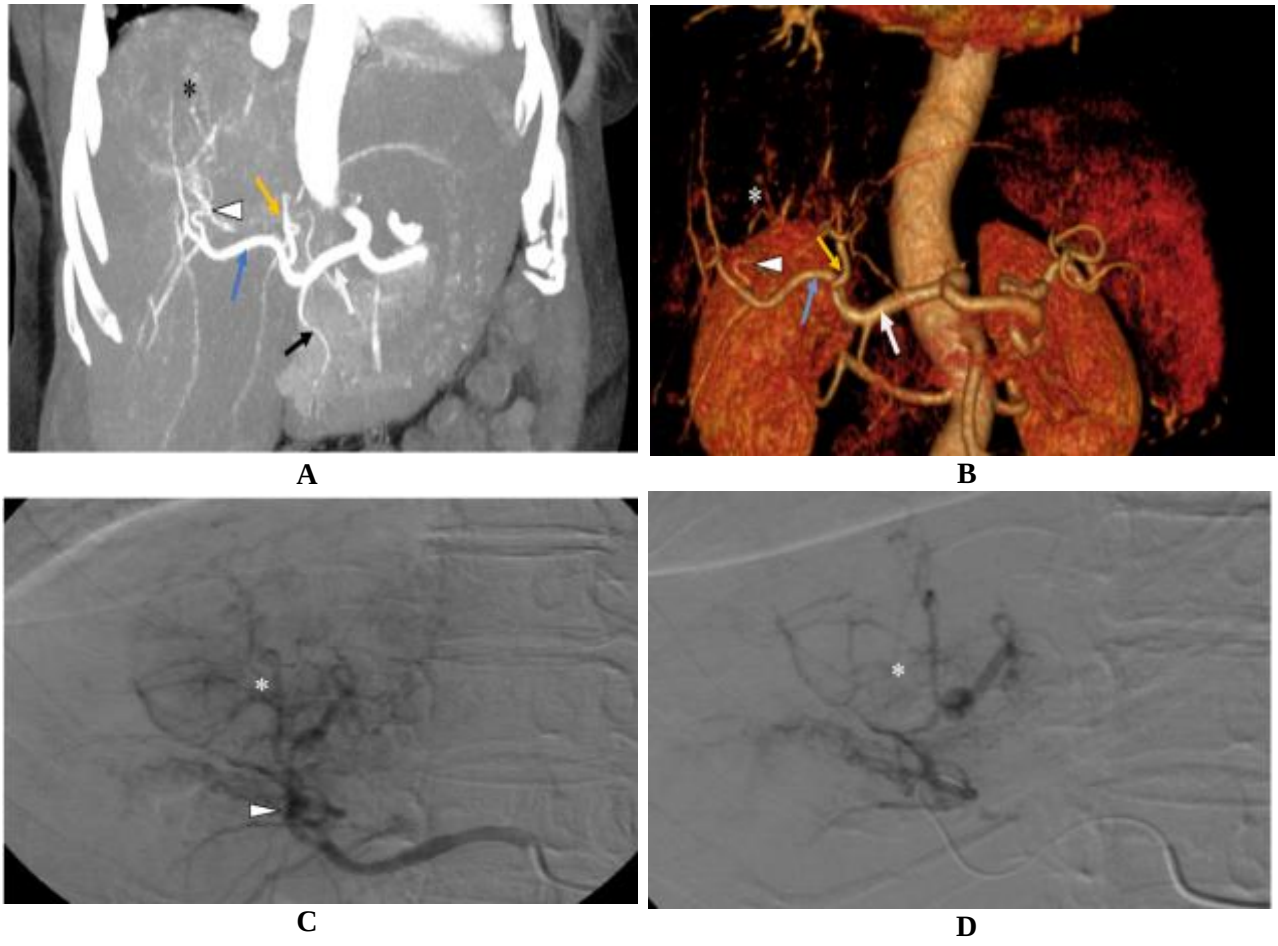

A **B**

C **D**

Case (1): Fig. A to D: Female patient aged 77 years old with de novo HCC focal lesion at right lobe segment VII measuring about 8x7cm. Coronal CT angiography with MIP reconstruction (A) and VR image (B) showing normal anatomy of hepatic artery: CHA (white arrow) gives GDA (black arrow) and then divides into RHA (blue arrow) and LHA (yellow arrow). Right lobe HCC (*) supplied from RPHA (arrowhead). DSA of RHA(C) and Selective DSA of the posterior division of RHA (D) showing tumoral blush (*) supplied from RPHA (arrowhead).

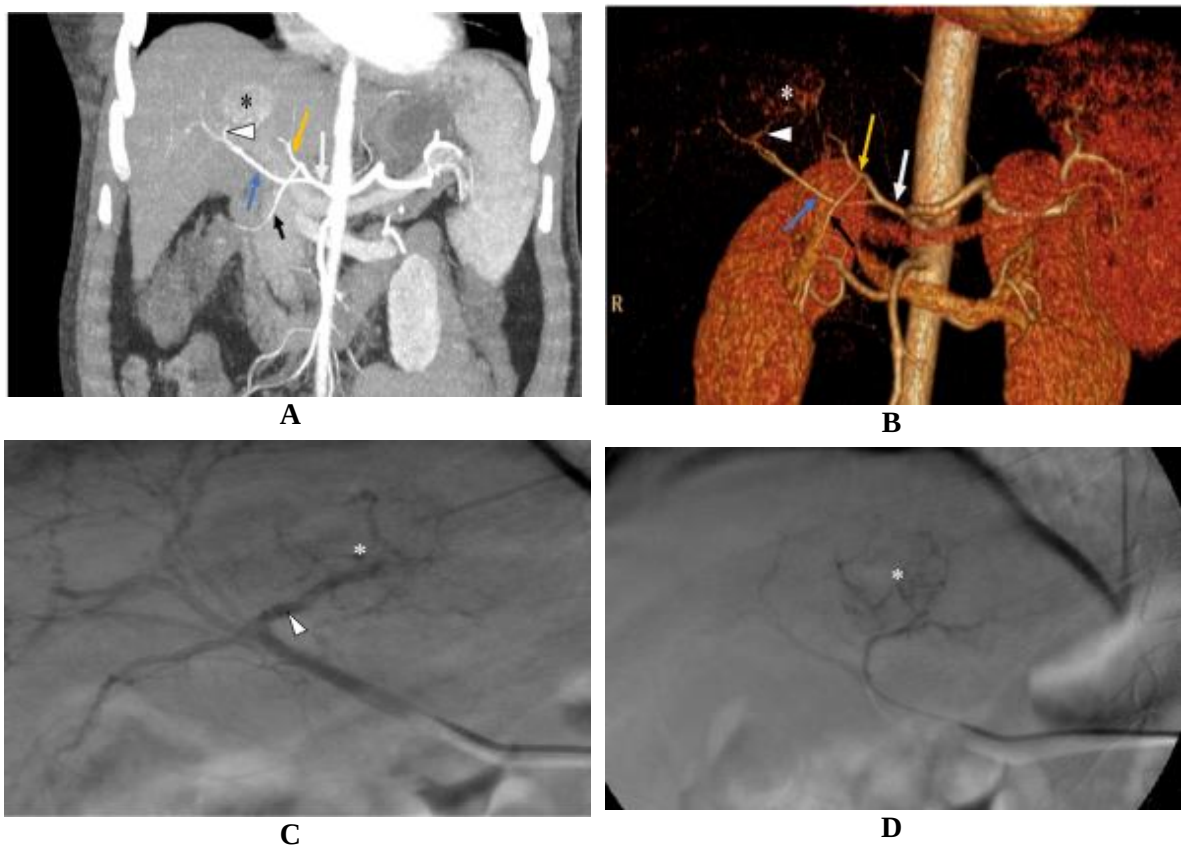

Case (2): Fig. A to D: Male patient aged 49 years old with de novo HCC focal lesion at left lobe segment IV measuring about 3x3 cm. Coronal CT angiography with MIP reconstruction (A), and VR image (B) showing early bifurcation of CHA (white arrow) into RHA (blue arrow) and LHA (yellow arrow). GDA (black arrow) originates from LHA. Left lobe HCC (*) with feeder artery (white arrowhead) from RHA. DSA of RHA left lobe focal lesion (*) with feeding artery (white arrowhead) from RHA (C). Selective DSA of the feeding artery of the focal lesion (*) (D).

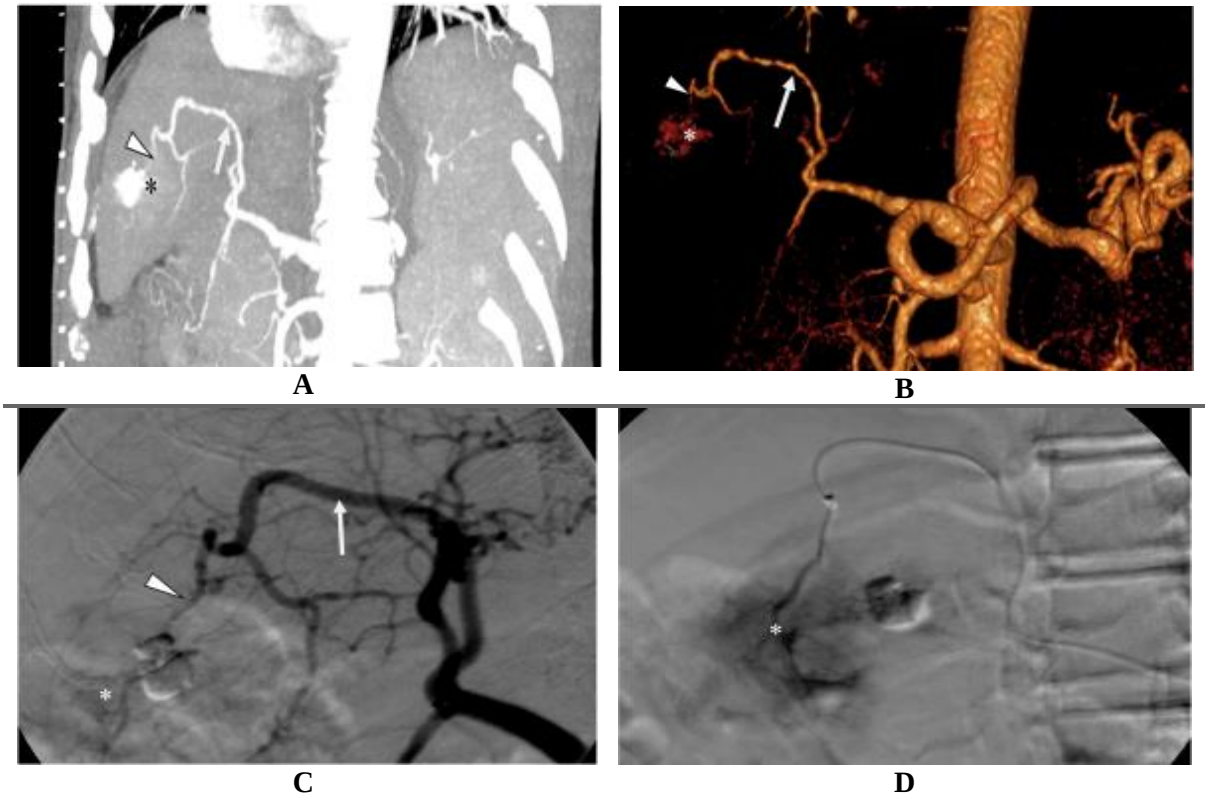

Case (3): Fig. A to D: Male patient aged 63 years old with previously chemoembolized HCC focal lesion at the right lobe segment VI measuring about 4x4 cm and still showing activity. Coronal oblique CT angiography with MIP reconstruction (A), VR image (B), and DSA of CHA (C) showing right lobe focal lesion (*), which was previously chemoembolized and still showing focal tumor blush (activity) with feeding artery (white arrowhead) from RPHA (white arrow). Selective DSA of the feeding artery of the right lobe focal lesion from RPHA (*) (D).

DISCUSSION

HCC is most commonly related to underlying hepatic cirrhosis, a premalignant state that is the irreversible consequence of many hepatic insults, such as inflammatory, toxic (alcohol), infectious (hepatitis), and metabolic processes like hemochromatosis [13]. TACE is locoregional chemotherapy delivered by a percutaneously inserted intravascular catheter advanced under imaging guidance as close to the tumour as possible in the hepatic artery [14].

Based on several studies, the prevalence of hepatic anatomical variations is very common ranging from 20-50% [15]. In our study, we found that 36 patients (72%) had normal anatomy of the hepatic artery and only 14 patients (28%) had anatomical variants. These findings match **Osman and Abdrabou [16] and Garg *et al.* [17]** who reported that normal anatomy of the hepatic artery was present in 74.2%, and 72% of cases respectively. Another study conducted by **Choi *et al.* [18]** found that the prevalence of overall aberrant hepatic arteries was 27.41%.

The most frequent variant in several studies based on Michel's classification, is type III, which is found in 6-15.5% of cases. The second most common is type II, documented in several studies between 2.5% and 10% [19]. In our trial, we found that the most frequent variant was type III presented in 6 cases (12%) and the second most common variant was type II presented in 4 cases (8%). These findings are in harmony with **Brasil *et al.* [20]** who found that type III was the most common anatomical variant presented in 10%.

Our study showed that CT angiography was highly accurate in assessing and evaluating the anomalies in the hepatic artery compared to the results of DSA; the accuracy of MIP and VRT was 100% and 94% respectively. These findings are congruent with the study of **Kim *et al.* [21]** who stated that the accuracy of MIP and VRT for assessment of hepatic artery anomalies was 100% and 91% respectively.

The current study reported that 48 lesions (70.6%) had single feeder arteries, 14 lesions (20.6%) had two feeder arteries and only 6 lesions (8.8%) had more than two feeder arteries. Therefore, the total number of feeders detected was 96 feeder arteries. These findings match with **Ohta *et al.* [22]** who reported that most of the lesions had single feeder arteries. However, **Abdelsalam *et al.* [23]** reported that (21.1%) of lesions had single feeder arteries, (35.1 %) of lesions had two feeder arteries, while (24.6%) of lesions had three feeder arteries, and only (19.3%) of lesions had four feeder arteries.

Regarding the source of feeder arteries in our study, 93 feeder arteries (96.9%) were from branches of hepatic arteries and 3 feeder arteries (3.1%) were extra-hepatic supplying 3 HCC lesions with residual activity; two feeder arteries were from right inferior phrenic artery and one feeder artery was from left internal mammary artery. These findings align with **Miyayama *et al.* [24]** who found that (1.9%) of detected feeder arteries were from inferior phrenic arteries. Also, the studies of **Moustafa *et al.* [25]** reported that the most common extra-hepatic supply for HCC is the right inferior phrenic artery.

Extra-hepatic supply of HCC is not uncommon and can impair the effectiveness of TACE therapy. Tumour size, tumour location, and the number of prior TACE treatments can all have an impact on the formation of EHC arteries. Large tumours over 5 cm and peripheral tumours have a greater prevalence of extra-hepatic supply [19].

In our study, there were two lesions in segment I; the first had a single feeder artery from the left hepatic artery (LHA) and the other lesion had two feeder arteries from the right hepatic artery (RHA) and right posterior hepatic artery (RPHA). This is supported by the study of **Kim *et al.* [26]** who stated that the caudate lobe has a variable arterial supply.

There were ten lesions in segment IV; 5 lesions were supplied by the segment IV artery that originated from LHA, 4 lesions were supplied by the segment IV artery that originated from RHA, and only one lesion with residual activity was supplied by the extra-hepatic feeding branch from left internal mammary artery. This is supported by **Saba *et al.* [27]** who stated that the segment IV artery takes origin from LHA in 55% of cases and from RHA in 31% of cases.

Concerning the accuracy of CT angiography for assessment of feeding arteries of HCC compared to results of DSA, our study found that MIP has more accuracy than VRT in detecting the feeder arteries. MIP revealed 84 feeder arteries (87.5%) while VRT revealed only 23 feeder arteries (24%). These findings match **Kim *et al.* [21]** who reported that the accuracy of MIP and VRT for detecting the feeder arteries of HCC was 77.8% and 22.2% respectively. This is explained by the fact that MIP uses the brightest voxels in a data set and projects them onto a 2D image, and other lower attenuation voxels are not well visualized. The thickness of the reconstructed volume of interest may be tailored to the researched region [28].

VR analyzes the content of each voxel within a data collection, assigns a particular color and transparency according to the voxel's underlying attenuation, and then shows the data in a 3D display. Consequently, VR depicts the vascular architecture and the connection of soft tissue, muscles, and bones, although occasionally it is difficult to differentiate tiny intrahepatic arteries from the hepatic parenchyma enhanced by the contrast, despite good calibration of the parameters of the VR [29].

Currently, 3D cone-beam CT angiography has shown a better outcome in comparison to DSA, and it may also provide a better outcome in comparison to MDCT angiography. MDCT angiography may provide information for the vascular map and identify the tumor-feeding vessel in cases scheduled for TACE with minimal effort [30].

CONCLUSION

Before chemoembolization, the hepatic arterial anatomy and its major variants must be checked on the pre-treatment CT scan. CT angiography with MIP demonstrated more accuracy and better quality of images than VRT for assessing HCC feeding arteries. It is anticipated that the use of CT angiography with MIP to evaluate the hepatic artery architecture and feeder arteries of HCC before TACE will reduce contrast material volume, procedure duration, and radiation exposure.

Conflict of interest: None declared.
Fund: Non-fundable.

REFERENCES

1. **Torre L, Siegel R, Ward E *et al.* (2016):** Global cancer incidence and mortality rates and trends—an update. Cancer Epidemiol Biomarkers Prev., 25:16-27.
2. **Singal A, Lampertico P, Nahon P (2020):** Epidemiology and surveillance for hepatocellular carcinoma: New trends. J Hepatol., 72: 250-61.
3. **European Association For The Study Of The Liver (2012):** EASL-EORTC clinical practice guidelines: management of hepatocellular carcinoma. J Hepatol., 56:908-43.
4. **Sharaf A, Elbadrawy E, Abdellatif A *et al.* (2022):** Frequency of hepatocellular carcinoma in cirrhotic patients after chronic hepatitis c infection treatment with direct-acting antivirals. Afro-Egypt J Infect Enem Dis., 12:16-23.
5. **Kumar Y, Sharma P, Bhatt N *et al.* (2016):** Transarterial therapies for hepatocellular carcinoma: a comprehensive review with current updates and future directions. Asian Pac J Cancer Prev., 17:473-8.
6. **Han K, Kim J (2015):** Transarterial chemoembolization in hepatocellular carcinoma treatment: Barcelona clinic liver cancer staging system. World J Gastroenterol., 21:10327-35.
7. **Cho Y, Choi J, Kwon H *et al.* (2023):** Transarterial chemoembolization for hepatocellular carcinoma: 2023 expert consensus-based practical recommendations of the Korean Liver Cancer Association. Korean J Radiol., 24:606-25.
8. **Bouvier A, Ozenne V, Aubé C *et al.* (2011):** Transarterial chemoembolization: effect of selectivity on tolerance, tumor response, and survival. European Radiology, 21:1719 - 26.
9. **Raman S, Fishman E (2012):** Advances in CT imaging of GI malignancies. Gastrointest Cancer Res., 5: 4-9.
10. **Liu P, Platt J (2014):** CT angiography in the abdomen: a pictorial review and update. Abdom Imaging, 39: 196-214.
11. **Ogawa K, Onishi H, Hori M *et al.* (2021):** Visualization of small visceral arteries on abdominal CT angiography using ultra-high-resolution CT scanner. Jpn J Radiol., 39:889-97.
12. **Molina D, DiMaio V (2012):** Normal organ weights in men: part II the brain, lungs, liver, spleen, and kidneys. Am J Forensic Med Pathol., 33:368-72.
13. **Ghouri Y, Mian I, Rowe J (2017):** Review of hepatocellular carcinoma: Epidemiology, etiology, and carcinogenesis. J Carcinog., 16:1-9.
14. **Ebeling Barbier C, Heindryckx F, Lennernäs H (2021):** Limitations and possibilities of transarterial chemotherapeutic treatment of hepatocellular carcinoma. Int J Mol Sci., 22: 23-29.
15. **Fonseca-Neto O, Lima H, Rabelo P *et al.* (2017):** Anatomic variations of hepatic artery: A study in 479 liver transplantations. Arq Bras Cir Dig., 30: 35-7.
16. **Osman A, Abdrabou A (2016):** Celiac trunk and hepatic artery variants: A retrospective preliminary MSCT report among Egyptian patients. Egypt J Radiol Nucl Med., 47: 1451-8.
17. **Garg S, Kumar K, Sahni D *et al.* (2020):** Anatomy of the hepatic arteries and their extrahepatic branches in the human liver: A cadaveric study. Ann Anat., 227:151-409.
18. **Choi T, Chung J, Kim H *et al.* (2021):** Anatomic variations of the hepatic artery in 5625 patients. Radiol Cardiothorac Imaging, 3:21-70.
19. **Roma S, D'Amato D, Ranalli T *et al.* (2019):** Vascular anomalies of the celiac trunk and implications in treatment of HCC with TACE. Description of a case and review of the literature. Radiol Case Rep., 14:1221-7.
20. **Brasil I, de Araujo I, Lima A *et al.* (2018):** Computed tomography angiography study of variations of the celiac trunk and hepatic artery in 100 patients. Radiol Bras., 51: 32-6.
21. **Kim I, Kim D, Kim K *et al.* (2014):** Feasibility of MDCT angiography for determination of tumor-feeding vessels in chemoembolization of hepatocellular carcinoma. J Comput Assist Tomogr., 38:742-6.
22. **Ohta K, Shimohira M, Hashizume T *et al.* (2019):** Identification of the feeding arteries of hepatocellular carcinomas by performing dual arterial phase CT during pre-transarterial chemoembolization angiography. Abdom Radiol (NY), 44:2276-82.
23. **Abdelsalam H, Emara D, Hassouna E (2022):** The efficacy of TACE; how can automated feeder software help? Egypt J Radiol Nucl Med., 53: 43-9.
24. **Miyayama S, Yamashiro M, Sugimori N *et al.* (2019):** Outcomes of patients with hepatocellular carcinoma treated with conventional transarterial chemoembolization using guidance software. J Vasc Interv Radiol., 30:10-8.
25. **Moustafa A, Abdel Aal A, Ertel N *et al.* (2017):** Chemoembolization of hepatocellular carcinoma with extrahepatic collateral blood supply: Anatomic and technical considerations. Radiographics, 37:963-77.
26. **Kim H, Miyayama S, Chung J (2019):** Selective chemoembolization of caudate lobe hepatocellular carcinoma: Anatomy and procedural techniques. Radiographics, 39:289-302.
27. **Saba L, Mallarini G (2011):** Anatomic variations of arterial liver vascularization: an analysis by using MDCTA. Surg Radiol Anat., 33: 559-68.
28. **Gümüs H, Bükte Y, Özdemir E *et al.* (2013):** Variations of the celiac trunk and hepatic arteries: a study with 64-detector computed tomographic angiography. Eur Rev Med Pharmacol Sci., 17:1636-41.
29. **Hennedige T, Anil G, Madhavan K (2014):** Expectations from imaging for pre-transplant evaluation of living donor liver transplantation. World J Radiol., 6:693-707.
30. **Diab I, Hassanein S, Mohamed H (2019):** Comparison between C-arm cone beam computed tomography and interventional angiography in transarterial chemoembolization of hepatocellular carcinoma. Egypt J Radiol Nucl Med., 50: 64-9.